The ubiquitin ligase UBE3B, disrupted in intellectual disability and absent speech, regulates metabolic pathways by targeting BCKDK

Solmi Cheon[a], Kiran Kaur[a], Nadine Nijem[a], Islam Oguz Tuncay[b], Pooja Kumar[a], Milan Dean[a], Jane Juusola[c], Maria J. Guillen-Sacoto[c], Emma Bedoukian[d], Lynne Ierardi-Curto[e], Paige Kaplan[e], G. Bradley Schaefer[f], Prashant Mishra[g], and Maria H. Chahrour[a,b,h,1]

[a]Eugene McDermott Center for Human Growth and Development, University of Texas Southwestern Medical Center, Dallas, TX 75390; [b]Department of Neuroscience, University of Texas Southwestern Medical Center, Dallas, TX 75390; [c]GeneDx Inc., Gaithersburg, MD 20877; [d]Roberts Individualized Medical Genetics Center, Children's Hospital of Philadelphia, Philadelphia, PA 19104; [e]Division of Human Genetics and the Metabolic Disease Program, Children's Hospital of Philadelphia, Philadelphia, PA 19104; [f]Division of Genetics, University of Arkansas for Medical Sciences, Little Rock, AR 72205; [g]Children's Medical Center Research Institute, University of Texas Southwestern Medical Center, Dallas, TX 75390; and [h]Department of Psychiatry, University of Texas Southwestern Medical Center, Dallas, TX 75390

Edited by Arthur L. Beaudet, Baylor College of Medicine, Houston, TX, and approved January 4, 2019 (received for review October 31, 2018)

Kaufman oculocerebrofacial syndrome (KOS) is a recessive neurodevelopmental disorder characterized by intellectual disability and lack of speech. KOS is caused by inactivating mutations in *UBE3B*, but the underlying biological mechanisms are completely unknown. We found that loss of *Ube3b* in mice resulted in growth retardation, decreased grip strength, and loss of vocalization. The brains of *Ube3b*$^{-/-}$ mice had hypoplasia of the corpus callosum, enlarged ventricles, and decreased thickness of the somatosensory cortex. *Ube3b*$^{-/-}$ cortical neurons had abnormal dendritic morphology and synapses. We identified 22 UBE3B interactors and found that branched-chain α-ketoacid dehydrogenase kinase (BCKDK) is an in vivo UBE3B substrate. Since BCKDK targets several metabolic pathways, we profiled plasma and cortical metabolomes from *Ube3b*$^{-/-}$ mice. Nucleotide metabolism and the tricarboxylic acid cycle were among the pathways perturbed. Substrate-induced mitochondrial respiration was reduced in skeletal muscle but not in liver of *Ube3b*$^{-/-}$ mice. To assess the relevance of these findings to humans, we identified three KOS patients who had compound heterozygous *UBE3B* mutations. We discovered changes in metabolites from similar pathways in plasma from these patients. Collectively, our results implicate a disease mechanism in KOS, suggest that it is a metabolic encephalomyopathy, and provide an entry to targeted therapies.

intellectual disability | autism spectrum disorder | ubiquitination | BCKDK | UBE3B

Neurodevelopmental disorders (NDDs) affect ∼15% of children in the United States and pose significant societal and economic burdens (1–4). NDDs make up a clinically and genetically heterogeneous group of diseases that affect brain development and function and often other organs. Intellectual disability (ID) and autism spectrum disorder (ASD) are the most common forms of NDD (3, 5) and often coexist in the same individual. The two conditions have high heritability (6, 7), with a multitude of gene defects underlying disease (8–13). Kaufman oculocerebrofacial syndrome (KOS; MIM 244450) is an NDD characterized by severe ID, absence of speech, microcephaly, muscle hypotonia, and growth retardation (14). KOS is an autosomal recessive disorder caused by complete loss-of-function mutations in *UBE3B*, a gene encoding an uncharacterized HECT (homologous to E6AP carboxyl terminus) E3 ubiquitin ligase (14–19). Moreover, we identified a recessive missense *UBE3B* mutation in a family with ASD (20).

UBE3B is a member of the proteasome pathway that functions in protein turnover and ubiquitin-mediated signaling. Mutations in several ubiquitin ligases result in ID and/or ASD, including *UBE3A* in Angelman syndrome (21), *HUWE1* in syndromic X-linked ID (22), *PSMD12* in ID (23), and *UBE3C*, which has recently been associated with ASD risk (24). How disruption of *UBE3B* gives rise to neurodevelopmental phenotypes, the disease mechanisms in KOS, and the specific substrates of UBE3B that mediate these mechanisms are not known. To address these questions, we sought to investigate the neurobehavioral consequences of losing UBE3B and identify its substrates.

Results

***Ube3b* Knockout Mice Have Growth Retardation and Absent Vocalization.** To understand the physiological function of UBE3B and investigate the mechanisms responsible for the phenotypes seen in KOS, we generated *Ube3b*$^{-/-}$ mice (*SI Appendix*, Fig. S1). *Ube3b*$^{-/-}$ mice were born in expected Mendelian ratios (*SI Appendix*, Fig. S1*D*), and had a ∼30% reduction in body weight and a ∼10% reduction in length compared with control littermates (Fig. 1*A*). In addition, the weights of brain and testes were reduced in *Ube3b*$^{-/-}$ mice, while the ratios of organ to body weight were unchanged (*SI Appendix*, Fig. S2). Heterozygous *Ube3b*$^{+/-}$ mice were indistinguishable from wild-type (WT) littermates.

Given the complete lack of speech seen in the majority of KOS patients—∼89%, including the three patients reported

Significance

UBE3B is a ubiquitin ligase disrupted in severe neurodevelopmental diseases (NDDs). Mechanistic studies on the function of UBE3B and its substrates have been lacking. Here, we show that deletion of *Ube3b* in mice causes neuroanatomical, behavioral, and metabolic abnormalities. Moreover, we identify BCKDK as a substrate UBE3B ubiquitinates. *BCKDK* is mutated in a spectrum of NDDs, and encodes a kinase that regulates several metabolic pathways. We show that *UBE3B* mutations are associated with metabolic disturbances in plasma from patients. Our findings place two NDD genes, *UBE3B* and *BCKDK*, in the same pathway, functionally validate the role of *UBE3B* in human disease, and identify both a disease mechanism in patients with *UBE3B* mutations and the downstream substrate that mediates this mechanism.

Author contributions: P.M. and M.H.C. designed research; S.C., K.K., N.N., I.O.T., P. Kumar, M.D., J.J., M.J.G.-S., E.B., L.I.-C., P. Kaplan, G.B.S., P.M., and M.H.C. performed research; S.C., K.K., N.N., I.O.T., P. Kumar, M.D., P.M., and M.H.C. analyzed data; M.H.C. wrote the paper; J.J., M.J.G.-S., E.B., and G.B.S. referred subjects; and L.I.-C., P. Kaplan, and G.B.S. performed clinical phenotyping of subjects.

The authors declare no conflict of interest.

This article is a PNAS Direct Submission.

[1]To whom correspondence should be addressed. Email: maria.chahrour@utsouthwestern.edu.

This article contains supporting information online at www.pnas.org/lookup/suppl/doi:10.1073/pnas.1818751116/-/DCSupplemental.

Published online February 11, 2019.

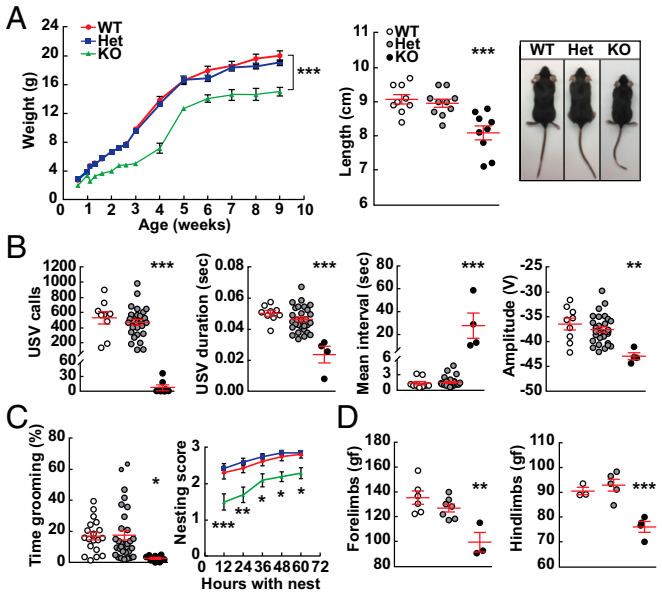

Fig. 1. Loss of *Ube3b* results in growth retardation, lack of vocalization, and muscle weakness. (*A*) *Ube3b*$^{-/-}$ knockout (KO) mice show significant reduction in weight and length versus WT or *Ube3b*$^{+/-}$ (heterozygotes; Het) (weight: ***$P < 0.0001$, two-way ANOVA; $n = 5$–18 WT, 7–37 Het, 5–12 KO; nose-to-rump length: ***$P = 0.0003$, one-way ANOVA; $n = 9$ WT, 10 Het, 9 KO). (*B*) KO mice have severe reduction in the number of and changes in duration, interval, and amplitude of USVs (***$P < 0.0001$, **$P < 0.0025$; $n = 9$ WT, 29 Het, 8 KO; duration, interval, amplitude: $n = 9$ WT, 29 Het, 4 KO). (*C*) KO mice spend less time grooming and their ability to construct nests is impaired (grooming: *$P = 0.0273$; nest building: ***$P < 0.0005$, **$P < 0.002$, *$P < 0.05$; $n = 16$–19 WT, 28–31 Het, 8–10 KO). (*D*) KO mice have reduced grip strength of both forelimbs and hindlimbs (***$P = 0.0008$, **$P = 0.0019$; $n =$ 3–6 WT, 5–7 Het, 3–4 KO). Values are mean ± SEM.

here (17)—we analyzed the ability of *Ube3b*$^{-/-}$ mice to emit ultrasonic vocalizations (USVs). Almost all *Ube3b*$^{-/-}$ mice had complete loss of USVs (Fig. 1*B*). The few mice that did vocalize had significantly fewer USVs and USV quality was altered compared with control littermates (Fig. 1*B* and *SI Appendix*, Fig. S3 *A* and *B*).

We measured self-grooming and marble burying to assess repetitive behaviors and found that *Ube3b*$^{-/-}$ mice performed significantly worse than control littermates in both assays (Fig. 1*C* and *SI Appendix*, Fig. S3*C*). The *Ube3b*$^{-/-}$ mice also performed poorly on the nest building test (Fig. 1*C*). Since patients with KOS have muscle hypotonia (14), we measured grip strength. We found that *Ube3b*$^{-/-}$ mice had reduced muscle strength in both their forelimbs and hindlimbs (Fig. 1*D*).

Loss of *Ube3b* Results in Dendritic and Synaptic Abnormalities. Human and mouse *Ube3b* is expressed ubiquitously, with the highest expression in testis (*SI Appendix*, Fig. S4). The targeted locus in *Ube3b*$^{+/-}$ mice included a lacZ cassette enabling us to characterize Ube3b expression by β-gal staining. We found that Ube3b expression in brain was highest in the hippocampus and cortical layers II/III and V (*SI Appendix*, Fig. S5), which are regions important in cognition and memory. The brains of *Ube3b*$^{-/-}$ mice had a hypoplastic corpus callosum and enlarged ventricles (*SI Appendix*, Fig. S6). In addition, the thickness of the primary somatosensory cortex was decreased, while the thickness of the primary motor cortex was preserved (*SI Appendix*, Fig. S6).

To assess the role of *Ube3b* in neuronal development, we measured dendritic complexity, length, and spine density in vivo by Golgi-Cox staining of brains from *Ube3b*$^{-/-}$ and WT littermates. Sholl analysis revealed reduced dendritic complexity in cortical neurons from *Ube3b*$^{-/-}$ mice (Fig. 2 *A*–*C*), which was more pronounced in the caudal cortex (Fig. 2 *A*–*C*). Cortical neurons from *Ube3b*$^{-/-}$ mice had significant reduction in dendritic length (~34–42% decrease) and dendritic spine density (~28–31% decrease) compared with neurons from WT littermates (Fig. 2 *B* and *C*).

We isolated primary neurons from the cortices of *Ube3b*$^{-/-}$ mice and WT littermates. We transfected the neurons with a GFP-expressing plasmid to outline neuronal morphology and immunostained them with presynaptic (synapsin I), postsynaptic [postsynaptic density protein 95 (PSD95)], and inhibitory synapse [vesicular GABA transporter (VGAT)] markers. Cortical neurons from *Ube3b*$^{-/-}$ mice had a ~24% decrease in presynaptic (synapsin I) puncta, a ~33% increase in postsynaptic (PSD95) puncta (Fig. 2*D*), and a ~50% increase in VGAT puncta (Fig. 2*E*). Collectively, these results suggest a role for UBE3B in neuronal morphogenesis and differentiation.

Proteomics Identifies UBE3B Interactors. To identify proteins that physically interact with UBE3B and are candidate substrates, we generated a HEK293T cell line (HEK293T$^{\text{UBE3B-HA}}$) that stably expresses a tagged version of UBE3B (UBE3B-HA). This was required since no anti-UBE3B antibodies were available that were suitable for immunoprecipitation. We immunoprecipitated UBE3B-HA and performed mass spectrometry (MS) to detect its interactors. Spectral counts for unique proteins identified by

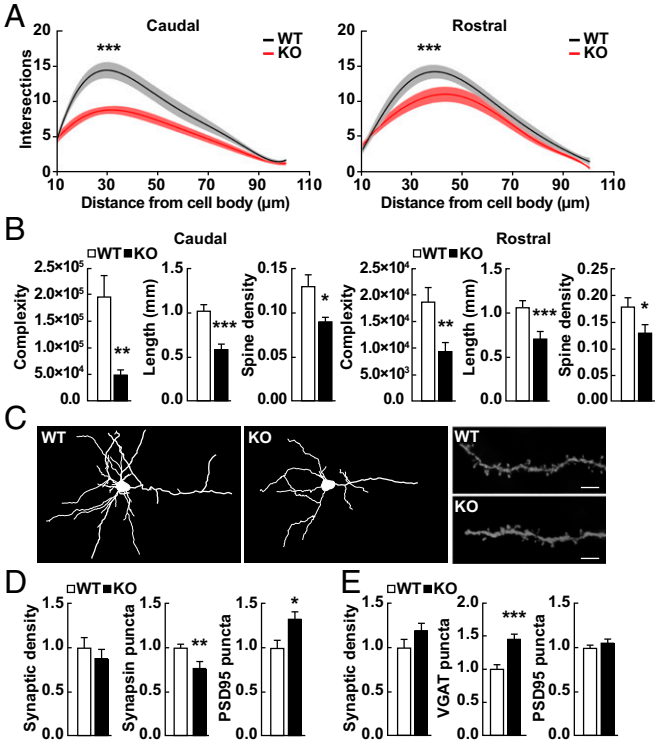

Fig. 2. *Ube3b* knockout mice have impaired dendritic morphogenesis and altered synapses. (*A*) Sholl analysis from Golgi-Cox–stained neurons reveals a reduction in dendritic complexity of cortical neurons from KO versus WT (***$P < 0.0001$, two-way ANOVA; $n = 13$–15 WT, 10–15 KO). (*B*) Golgi-Cox staining shows significantly reduced dendritic complexity, length, and spine density in neurons from the caudal and rostral cortex of KO versus WT. Data were obtained from basal dendrites of cortical layer II/III neurons (caudal: *$P = 0.0235$, **$P = 0.0029$, ***$P < 0.0001$; rostral: *$P = 0.0355$, **$P = 0.0057$, ***$P = 0.0029$; $n = 13$–15 WT, 10–15 KO). (*C*, *Left*) Representative tracings of Golgi-Cox–stained cortical layer II/III neurons and (*C*, *Right*) of their dendritic segments. (Scale bars, 5 μm.) (*D*) Primary cortical neurons from KO have less synapsin I puncta and more PSD95 puncta versus WT (*$P = 0.0213$, **$P = 0.004$; $n = 20$ WT, 10 KO). (*E*) Primary cortical neurons from KO have increased VGAT puncta versus WT (***$P = 0.0002$; $n = 10$ WT, 20 KO).

MS were analyzed using the Comparative Proteomic Analysis Software Suite (CompPASS) as previously described (25). We identified 22 high-confidence candidate interacting proteins (HCIPs) (Table 1). Three of the HCIPs—BCKDK, BCKDHA, and DBT—function in BCAA metabolism (Fig. 3*A*). The second step in BCAA metabolism catalyzed by the branched-chain α-ketoacid dehydrogenase complex (BCKDC) is irreversible and rate limiting (26). BCKDC has three components: (*i*) branched-chain α-ketoacid decarboxylase, a heterotetramer of two branched-chain α-ketoacid dehydrogenase E1 alpha (BCKDHA) and two beta (BCKDHB) subunits, (*ii*) dihydrolipoamide branched-chain transacylase (DBT), and (*iii*) dihydrolipoamide dehydrogenase (DLD) (Fig. 3*A*). Thus, we found that two of the three catalytic subunits of BCKDC interact with UBE3B. BCKDK, another HCIP, is the kinase that regulates activity of the complex by phosphorylating and inactivating BCKDHA. Mutations in *BCKDK* cause ID, ASD, and epilepsy (27), while mutations in *BCKDHA* or *DBT* cause maple syrup urine disease (MSUD; MIM 248600), a disorder characterized by ID, developmental delay, and a maple syrup odor to urine (28).

We confirmed that BCKDK and DBT physically interact with UBE3B using coimmunoprecipitation in HEK293T$^{UBE3B\text{-}HA}$ (*SI Appendix*, Fig. S7*B*). To determine whether UBE3B ubiquitinates BCKDK, BCKDHA, or DBT, we performed denaturing immunoprecipitation. We transfected Myc-BCKDK into HEK293T$^{UBE3B\text{-}HA}$ and into HEK293T cells that do not express UBE3B. We then immunoprecipitated Myc-BCKDK to isolate it without any interacting proteins and performed Western blot analysis with both anti-Myc and anti-ubiquitin antibodies. BCKDK was ubiquitinated in cells expressing UBE3B (Fig. 3*B*) and this ubiquitination was enhanced by treatment with the proteasome inhibitor bortezomib (Fig. 3*B*). Using the same assay in HEK293T$^{UBE3B\text{-}HA}$ cells and WT tissue, we did not detect ubiquitination of BCKDHA or DBT (*SI Appendix*, Fig. S8 *A*–*C*). The data suggest that UBE3B ubiquitinates BCKDK but not BCKDHA or DBT.

Table 1. Proteomics identifies UBE3B interactors and candidate substrates

Symbol	Name	NWD score	*Z* score
BCKDHA	Branched-chain α-ketoacid dehydrogenase E1, alpha polypeptide	0.77	8.91
BCKDK	Branched-chain α-ketoacid dehydrogenase kinase	1.03	9.38
CALM3	Calmodulin 3	2.13	9.63
CEP55	Centrosomal protein 55	1.54	10.42
CPNE7	Copine 7	2.18	11.00
DBT	Dihydrolipoamide branched-chain transacylase	3.39	11.49
DYNLRB2	Dynein light-chain roadblock-type 2	1.09	8.25
GTPBP8	GTP-binding protein 8	2.18	11.00
LAMC1	Laminin subunit gamma 1	3.09	11.71
LMNA	Lamin A/C	1.06	3.87
PAIP1	Poly(A) binding protein interacting protein 1	1.09	8.25
PPP3R1	Protein phosphatase 3 regulatory subunit B, alpha	2.18	11.00
PPP4R3C	Protein phosphatase 4 regulatory subunit 3C	2.18	11.00
PSMA1	Proteasome subunit alpha 1	1.78	10.98
PSMA3	Proteasome subunit alpha 3	1.22	10.98
PSMB1	Proteasome subunit beta 1	1.96	11.48
PSMB2	Proteasome subunit beta 2	1.89	9.55
PSMB3	Proteasome subunit beta 3	2.70	11.44
PSMB4	Proteasome subunit beta 4	3.06	11.57
PSMB7	Proteasome subunit beta 7	4.36	11.68
SF3A1	Splicing factor 3a subunit 1	1.04	0.55
UBE3B	Ubiquitin protein ligase E3B	21.49	11.66
ZBED4	Zinc finger BED-type containing 4	3.09	11.71

NWD, normalized weighted D-score.

BCKDK Is an in Vivo Substrate of UBE3B. *Ube3b* is expressed in three tissues that are the major sites of BCAA metabolism: brain, liver, and skeletal muscle (*SI Appendix*, Figs. S1, S4, and S5). To determine the effect of inactivating *Ube3b* on levels of BCKDK, BCKDHA, and DBT in these tissues, we compared levels of these proteins in *Ube3b*$^{-/-}$ mice and control littermates. BCKDK levels were significantly higher in all three tissues of *Ube3b*$^{-/-}$ mice (Fig. 3*C*), which is consistent with BCKDK being an in vivo substrate of Ube3b. In contrast, no differences were seen in the levels of BCKDHA in tissues from *Ube3b*$^{-/-}$ mice. DBT levels were increased in skeletal muscle but not cortex or liver of *Ube3b*$^{-/-}$ mice (Fig. 3*C*).

To confirm that changes in BCKDK protein levels were due to a difference in posttranslational modification, we compared *Bckdk* transcript levels in tissues from *Ube3b*$^{-/-}$ mice and control littermates. We found no differences in *Bckdk* mRNA levels between genotypes (*SI Appendix*, Fig. S8*D*), whereas *Dbt* transcript levels were higher in *Ube3b*$^{-/-}$ skeletal muscle (*SI Appendix*, Fig. S8*D*). Thus, the observed increase in DBT protein levels (Fig. 3*C*) was due to transcriptional changes in *Dbt* expression.

UBE3B Regulates Several Metabolic Pathways. Since BCKDK phosphorylates key enzymes in several metabolic pathways, including BCKDHA, acetyl-CoA carboxylase alpha (ACC1), ATP citrate lyase (ACL), nicotinamide adenine dinucleotide kinase (NADK), and tyrosine aminotransferase (TAT) (29), we investigated whether changes in BCKDK levels resulted in changes in levels of tissue metabolites in *Ube3b*$^{-/-}$ mice. We profiled the relative abundance of over 200 metabolites in plasma and cortical tissue from WT and *Ube3b*$^{-/-}$ mice. The metabolites represented pathways from amino acid biogenesis, the TCA cycle, glycolysis, the pentose phosphate pathway (PPP), and nucleotide metabolism, among others (Dataset S1). We detected 138 and 139 metabolites in plasma and cortex, respectively (Dataset S2 *A* and *B*), that clustered by genotype (Fig. 4*A*). Loss of UBE3B led to significant changes in levels of several metabolites in plasma and cortex (Fig. 4*C* and *SI Appendix*, Figs. S9 and S10). Metabolites that changed the most in *Ube3b*$^{-/-}$ plasma compared with WT were those belonging to the TCA cycle and nucleotide metabolism (*SI Appendix*, Fig. S9). In the cortex, significant changes were found in metabolites belonging to these two pathways as well as those from amino acid metabolism and glycolysis (*SI Appendix*, Fig. S10).

Given that several of the pathways implicated by the metabolomics survey occur in mitochondria and that UBE3B localizes to the mitochondria as well as the cytoplasm (30), we analyzed mitochondrial morphology in neural stem cells isolated from *Ube3b*$^{-/-}$ mice and control littermates. We found no changes in mitochondrial morphology (*SI Appendix*, Fig. S11). Thus, the changes observed using metabolomics did not appear to be due to a more generalized alteration in mitochondrial structure.

To examine the enzymatic activity of BCKDC, we measured branched-chain α-ketoacid–induced mitochondrial respiration in brain, liver, and skeletal muscle of WT and *Ube3b*$^{-/-}$ mice. We found that mitochondria-enriched liver fractions from WT and *Ube3b*$^{-/-}$ mice showed no significant difference in respiratory activity in the presence of the BCKDC substrate α-ketoisovaleric acid (α-KIV), the α-ketoacid of valine (Fig. 4*E*). No detectable BCKDC activity was observed in brain mitochondria (*SI Appendix*, Fig. S12). In contrast, we found that mitochondria-enriched fractions from skeletal muscle of *Ube3b*$^{-/-}$ mice had a ∼2.55-fold reduction in α-KIV–induced respiration (Fig. 4*E*).

These data suggest that BCKDK accumulation leads to reduced BCKDC activity only in skeletal muscle in *Ube3b*$^{-/-}$ mice. Consistent with this finding, phospho-BCKDHA was increased in skeletal muscle but not liver of *Ube3b*$^{-/-}$ mice (Fig. 4*F*). Taken together, the metabolic aberrations found in the tissues of *Ube3b*$^{-/-}$

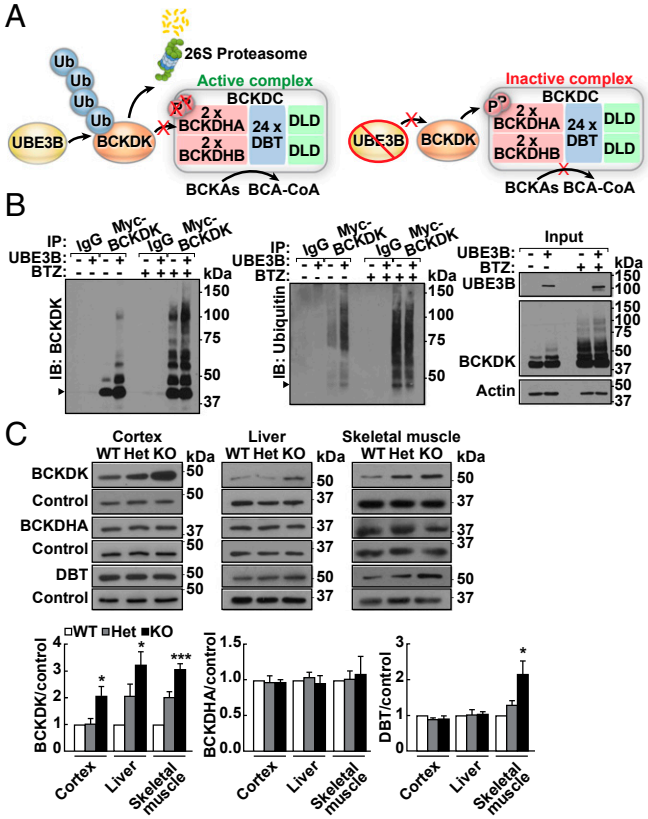

Fig. 3. UBE3B ubiquitinates BCKDK and targets it for degradation. (*A*) BCKDC catalyzes the oxidative decarboxylation of branched-chain α-ketoacids (BCKAs), derivatives of BCAAs, into branched-chain acyl-CoA (BCA-CoA) species. UBE3B ubiquitinates BCKDK, targeting it for degradation. In the absence of UBE3B, BCKDK accumulates, resulting in increased phosphorylation of BCKDC and a decrease in complex activity. (*B*) UBE3B ubiquitinates BCKDK. HEK293T (–) or HEK293T stable cells expressing UBE3B-HA (+) were transfected with Myc-BCKDK and treated with bortezomib (BTZ) (+) or vehicle (–). Lysates were subject to denaturing immunoprecipitation (IP) with anti-Myc or IgG agarose, and IP fractions were analyzed by anti-Myc (*Left*) or anti-ubiquitin immunoblotting (IB) (*Right*). Arrowheads point to BCKDK (*Left*) and its 46-kDa band (*Right*). Higher molecular-weight bands correspond to ubiquitinated forms of BCKDK. Input fractions were analyzed by anti-Ube3b, anti-BCKDK, or anti-actin IB. (*C*, *Top*) Western blot of cortex, liver, or skeletal muscle of WT, Het, or KO mice shows accumulation of BCKDK but not BCKDHA in KO tissues. DBT accumulates in KO skeletal muscle but not in cortex or liver. (*C*, *Bottom*) Western blot quantifications. Values are mean ± SEM (BCKDK: cortex $*P = 0.0298$, liver $*P = 0.0162$, skeletal muscle $***P = 0.0003$; DBT: $*P = 0.0235$; for each tissue $n = 3$–4 per genotype). Control refers to IB with anti-actin (cortex) or anti-GAPDH (glyceraldehyde-3-phosphate dehydrogenase; liver, skeletal muscle).

mice coupled with the identification of BCKDK as a UBE3B substrate suggest that KOS may be a metabolic encephalomyopathy with primary effects on multiple target organs.

Altered Plasma Metabolomic Profile in Patients with KOS. As part of our ongoing studies to understand the mechanisms underlying KOS, we identified two families where clinical whole-exome sequencing (WES) revealed pathogenic variants in *UBE3B*. The proband from the first family (UB-1) was a boy who was initially identified in infancy (UB-1–3). He had developmental delay, ID, lack of speech, microcephaly, hypotonia, and feeding difficulty (Table 2). WES revealed that he was a compound heterozygote for two missense mutations in *UBE3B*: p.Q642R (maternally inherited) and p.D963N (paternally inherited). The second family (UB-2) had two affected boys with KOS who were diagnosed at ages 3 and 6 (UB-2–3 and UB-2–4). The two brothers had severe ID, lack of speech, microcephaly, hypoplastic corpus callosum, and feeding difficulty (Table 2). Both siblings were compound heterozygotes for mutations in *UBE3B*: a maternally inherited frameshift mutation and a paternally inherited splice acceptor mutation (Table 2). We validated the mutations using Sanger sequencing and determined segregation of the mutations in both families (Fig. 5 *A* and *B*).

Western blot of lysates from lymphoblastoid cell lines showed a complete loss of UBE3B in the two affected siblings from family UB-2 (UB-2–3 and UB-2–4) compared with unaffected controls (Fig. 5*C*). This suggests that these mutations result in nonsense-mediated mRNA decay. No change was seen in UBE3B level in the other proband (UB-1–3) compared with unaffected controls

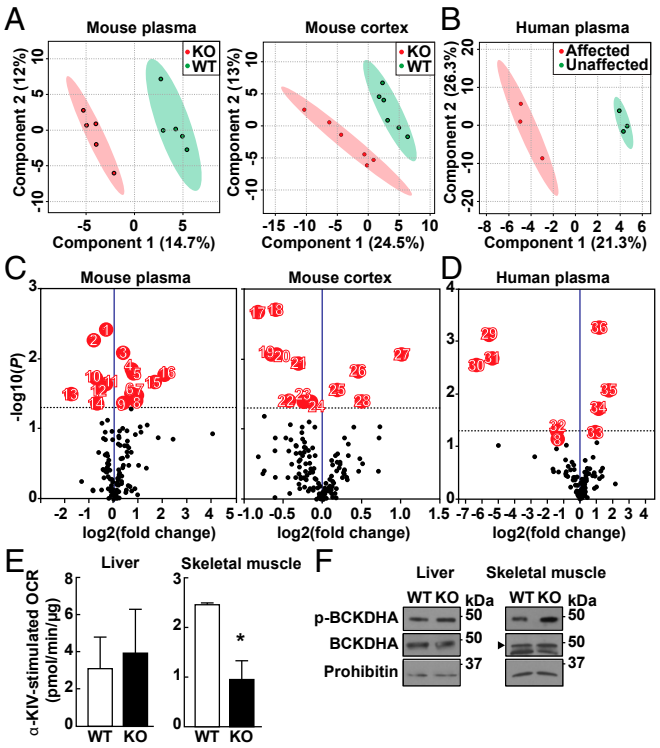

Fig. 4. Metabolic perturbations following loss of *Ube3b*. Metabolomics profiling from plasma and cortex of WT and KO mice ($n = 5$–6 WT, 5–6 KO) (*A*) and from plasma of KOS patients ($n = 3$: UB-1–3, UB-2–3, UB-2-4) and unaffected individuals ($n = 3$: UB-1–2, UB-2–1, UB-2-2) (*B*). Partial least squares discriminant analysis of metabolomics data. Volcano plots of metabolites altered in KO versus WT (*C*) and in affected versus unaffected individuals (*D*). Metabolites demonstrating significant changes in abundance are indicated in red, numbered, and individually plotted in *SI Appendix*, Figs. S9, S10, and S13. Dotted line represents $P < 0.05$. Mouse plasma (1: 4-hydroxybenzoic acid, 2: stearoylcarnitine, 3: pyridoxine, 4: uracil, 5: L-homoserine, 6: D-glutamic acid, 7: citric acid, 8: D-2-hydroxyglutaric acid, 9: thymidine, 10: tetradecanoylcarnitine, 11: choline, 12: 1-methyladenosine, 13: creatinine, 14: 1-methylnicotinamide, 15: S-adenosylhomocysteine, 16: spermidine), mouse cortex (17: niacinamide, 18: D-glucose, 19: L-lysine, 20: AICAR, 21: adenine, 22: propionylcarnitine, 23: cis-aconitic acid, 24: pipecolic acid, 25: shikimic acid, 26: 4-hydroxyproline, 27: phosphorylcholine, 28: urea), human plasma (29: guanine, 30: glucose-6-phosphate, 31: NAD, 32: adenosine, 33: creatine, 34: 5-aminolevulinic acid, 35: L-kynurenine, 36: 4-hydroxyproline). (*E*) α-KIV-induced respiration measured from liver and skeletal muscle mitochondria shows a ~2.55-fold reduction in skeletal muscle from KO versus WT ($*P = 0.0145$; $n = 3$ WT, 3 KO). Values are mean ± SEM. (*F*) Western blot of liver and skeletal muscle mitochondrial fractions shows increased phosphorylation of BCKDHA in skeletal muscle but not in liver from KO versus WT. Arrowhead points to BCKDHA band. Representative immunoblots from three independent experiments ($n = 3$ WT, 3 KO).

Table 2. Clinical phenotype of patients with *UBE3B* mutations

Patient	UB-1–3	UB-2–3	UB-2–4
Sex	Male	Male	Male
Age, y	20	11	8
Nucleotide change	c.1925 A>G c.2887 G>A	c.256delC c.941–1 G>A	c.256delC c.941–1 G>A
Amino acid change	p.Gln642Arg p.Asp963Asn	p.Leu86TyrfsX19 IVS11-1 G>A	p.Leu86TyrfsX19 IVS11-1 G>A
MAF (percentage)	NP 0.0137	0.0016 NP	0.0016 NP
Weight (percentile)	< first	< fifth	third
Head circumference (percentile)	< 0.01	< fifth	< fifth
DD	+	+	+
ID	+	+	+
Absent speech	+	+	+
Seizures	–	–	+
Muscle hypotonia	+	+	+
Feeding difficulties	+	+	+
Facial dysmorphisms	+	+	+
Abnormal MRI	+	NR	NR

All findings reported at latest examination. Mutations are compound heterozygous and are reported on human genome GRCh37/hg19 coordinates and RefSeq transcript NM_130466.3. DD, developmental delay; ID, intellectual disability; MAF, minor allele frequency in gnomAD; NP, not present; NR, not reported.

(Fig. 5*C*). It is possible that the missense mutations in UB-1–3 alter protein function or subcellular localization.

We profiled metabolite levels in plasma from the affected (UB-1–3, UB-2–3, UB-2–4) and unaffected (UB-1–2, UB-2–1, UB-2–2) individuals. We found that affected family members had differences in the abundance of 109 metabolites (Dataset S2*C*) that clustered by genotype (Fig. 4*B*). Several metabolites were significantly altered in plasma of affected individuals (Fig. 4*D* and *SI Appendix*, Fig. S13) and belonged to amino acid and nucleotide metabolism pathways, glycolysis and TCA cycle, energy metabolism, and heme biosynthesis (*SI Appendix*, Fig. S13).

Discussion

In this study. we identified a role for UBE3B in neuronal development and behavior, discovered an in vivo substrate for UBE3B, and gained insight into the disease mechanism in KOS. *Ube3b*$^{-/-}$ mice recapitulate phenotypes of KOS patients—namely, reduced growth, brain size, and muscle strength; lack of vocalization; and hypoplastic corpus callosum. *Ube3b*$^{-/-}$ mice also have enlarged ventricles and decreased thickness of the somatosensory cortex. We found that *Ube3b* is expressed in the hippocampal pyramidal layer and cortical layers II/III and V, among other brain regions, and identified a role for UBE3B in dendritic morphogenesis. In addition, *Ube3b*$^{-/-}$ cortical neurons showed a reduction in the presynaptic marker synapsin I and an increase in the postsynaptic marker PSD95, suggesting that these neurons are less mature and that loss of *Ube3b* may affect vesicle organization at synaptic terminals. *Ube3b*$^{-/-}$ cortical neurons had abnormalities in the number of VGAT-positive inhibitory synaptic puncta, suggesting delayed maturation of inhibitory neurons.

We identified several UBE3B interactors, including calmodulin-regulated protein phosphatase PPP3R1 (the calcium-binding subunit of calcineurin), a calmodulin, a calcium-dependent lipid-binding protein, a centrosomal protein that regulates cytokinesis, multiple proteasome subunits, and three members of the BCAA metabolism pathway (BCKDK, BCKDHA, and DBT). We found that UBE3B ubiquitinates BCKDK and targets it for degradation by the proteasome. BCKDK was initially identified as the kinase that phosphorylates BCKDHA, thus inactivating BCKDC. However, a recent study identified additional phosphorylation targets of BCKDK, including enzymes that function in lipogenesis (ACL), tyrosine transamination (TAT), and phosphorylation of nicotinamide adenine dinucleotide (NAD; NADK) (29). NADK phosphorylation of NAD generates NADP, which in turn enters the PPP to generate NADPH (the reduced form of NADP) and precursors for nucleotide biosynthesis. ATP-citrate lyase (ACL) is a key enzyme in lipogenesis, a process critical for neuronal differentiation (31). BCKDK accumulation may disrupt the regulation of lipogenesis in developing neurons of *Ube3b*$^{-/-}$ mice. Complete loss-of-function mutations in *BCKDK* result in ID, ASD, and epilepsy (27). Importantly, duplications spanning the *BCKDK* locus, including those at chromosome 16p11.2, result in a spectrum of neurodevelopmental phenotypes comprising developmental delay, speech and language abnormalities, ID, ASD, and microcephaly (13, 32, 33). Thus, human genetics data, combined with our data from *Ube3b*$^{-/-}$ mice, suggest that BCKDK plays an important role in brain development and function, and that overexpression of *BCKDK* may underlie the neurodevelopmental phenotypes observed in patients with duplications spanning the locus.

Additionally, we report on the first posttranslational modification of BCKDK as a mechanism to regulate its levels. Loss of *Ube3b* resulted in BCKDK accumulation in cortex, liver, and skeletal muscle of *Ube3b*$^{-/-}$ mice. Metabolomics profiling revealed that this accumulation led to changes in the levels of several metabolites from nucleotide and amino acid metabolism pathways, glycolysis, and TCA cycle. Metabolomics profiling in plasma from KOS patients revealed similar metabolic changes. In *Ube3b*$^{-/-}$ plasma, levels of several TCA-cycle metabolites were increased (citric acid, 2-hydroxyglutaric acid, glutamic acid, and succinic acid), suggesting that the TCA cycle is disrupted. Levels of choline, a precursor of acetylcholine, were decreased in *Ube3b*$^{-/-}$ plasma, while phosphorylcholine levels were increased in *Ube3b*$^{-/-}$ cortex. In *Ube3b*$^{-/-}$ cortex, there was a decrease in levels of adenine, 5-aminoimidazole-4-carboxamide ribonucleotide (AICAR), and niacinamide, all part of nucleotide metabolism pathways. Purine metabolites were also reduced in plasma from KOS patients—specifically, guanine, adenosine, and NAD—the last of which also functions in a multitude of pathways. In addition, glucose 6-phosphate was significantly reduced in plasma from KOS patients. Inborn errors of purine metabolism represent

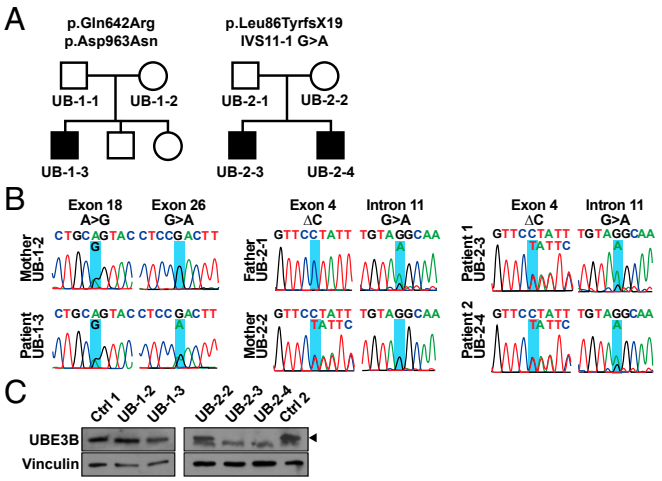

Fig. 5. Identification of recessive *UBE3B* mutations in two families with KOS. (*A*) Pedigrees of two families with compound heterozygous *UBE3B* mutations in three children affected by KOS. Shaded symbols indicate affected individuals. (*B*) Sanger-sequencing results for individuals from UB-1 and UB-2 confirmed segregation of *UBE3B* variants detected by clinical WES. (*C*) Western blot of lymphoblastoid cell line lysates from affected individuals (UB-1–3, UB-2–3, UB-2–4), unaffected family members (UB-1–2, UB-2–2), and two unrelated controls (Ctrl 1, Ctrl 2) show loss of UBE3B in affected individuals UB-2–3 and UB-2–4. Vinculin is a loading control. Arrowhead points to UBE3B band.

a rare class of disorders that result in a spectrum of clinical presentations, including severe neurological phenotypes (34).

Despite increased BCKDK in cortex, liver, and skeletal muscle from *Ube3b*$^{-/-}$ mice, we did not observe any significant changes in BCAAs or their metabolites in plasma and cortex from *Ube3b*$^{-/-}$ mice or in plasma from KOS patients (*SI Appendix*, Fig. S14). One explanation is that BCAA metabolites feed into other pathways (for example, the TCA cycle) and, since BCKDK regulates some of these pathways, there is a less pronounced effect on BCAA metabolism when BCKDK levels are elevated. On the other hand, in disorders where BCKDC subunits are defective (e.g., MSUD) or where BCKDK is deficient, there is a more direct effect on BCAA metabolism. However, when BCKDK levels are high, there is a significant effect on the TCA cycle and nucleotide metabolism. Another possibility is that the effect of BCKDK on BCAA metabolism is counteracted in brain and liver but not skeletal muscle of *Ube3b*$^{-/-}$ mice by the activity of PPM1K, the phosphatase that activates BCKDC.

Our findings that BCKDC activity is decreased specifically in skeletal muscle and that *Ube3b*$^{-/-}$ mice have reduced grip strength suggest that KOS is a multiorgan disease that includes a primary muscle deficit, classifying it as a metabolic encephalomyopathy. Furthermore, for the following reasons our data suggest that KOS is not a phenocopy of MSUD. In KOS, a partial defect in BCKDC activity is expected since BCKDC subunits are intact; thus, the consequences for BCAA metabolites are blunted in KOS. The decreased BCKDC activity observed in skeletal muscle of *Ube3b*$^{-/-}$ mice may be responsible for the observed myopathy, while the normal activity in liver prevents the metabolic changes seen in MSUD. Finally, the increase in BCKDK levels in KOS results in perturbations in multiple metabolic pathways. Collectively, this indicates that KOS and MSUD are not phenocopies and, as a consequence, the standard therapies implemented in patients with MSUD, such as diet modification and liver transplantation, may not work for patients with KOS. Treatment strategies designed to target BCKDK may have beneficial clinical effects in KOS.

Materials and Methods

The study was approved by the University of Texas Southwestern Medical Center (UTSW) Institutional Review Board, and written informed consent was obtained from participants. Phenotypes of affected individuals along with a detailed description of all materials and methods for generation of *Ube3b*$^{-/-}$ mice, analysis of neurobehavioral phenotypes, proteomics, and metabolomics are detailed in the *SI Appendix, SI Materials and Methods*.

ACKNOWLEDGMENTS. We are grateful to the families for their invaluable participation in our study. We thank Dr. R. Hammer and the UTSW Transgenic Core facility; Drs. J. W. Harper and L. Pontano-Vaites for mass spectrometry; Dr. R. DeBerardinis and L. Zacharias for metabolomics profiling; Dr. E. Plautz in the UTSW Neuro-Models Core Facility for the grip strength test; C. Burroughs for assistance with figures; and Dr. G. Konopka for her helpful comments on the manuscript. M.H.C. was supported by UTSW, a NARSAD Young Investigator grant from the Brain and Behavior Research Foundation, and a National Institute of Mental Health Grant (R21 MH115313).

1. Centers for Disease Control and Prevention (CDC) (2004) Economic costs associated with mental retardation, cerebral palsy, hearing loss, and vision impairment–United States, 2003. *MMWR Morb Mortal Wkly Rep* 53:57–59.
2. Boyle CA, et al. (2011) Trends in the prevalence of developmental disabilities in US children, 1997–2008. *Pediatrics* 127:1034–1042.
3. Developmental Disabilities Monitoring Network Surveillance Year 2010 Principal Investigators; Centers for Disease Control and Prevention (CDC) (2014) Prevalence of autism spectrum disorder among children aged 8 years–Autism and developmental disabilities monitoring network, 11 sites, United States, 2010. *MMWR Surveill Summ* 63:1–21.
4. Leigh JP, Du J (2015) Brief report: Forecasting the economic burden of autism in 2015 and 2025 in the United States. *J Autism Dev Disord* 45:4135–4139.
5. Le Hellard S, Steen VM (2014) Genetic architecture of cognitive traits. *Scand J Psychol* 55:255–262.
6. Colvert E, et al. (2015) Heritability of autism spectrum disorder in a UK population-based twin sample. *JAMA Psychiatry* 72:415–423.
7. Plomin R, DeFries JC, Knopik VS, Neiderhiser J (2013) *Behavioral Genetics* (Worth Publishers, New York), 6th Ed.
8. Betancur C (2011) Etiological heterogeneity in autism spectrum disorders: More than 100 genetic and genomic disorders and still counting. *Brain Res* 1380:42–77.
9. Neale BM, et al. (2012) Patterns and rates of exonic de novo mutations in autism spectrum disorders. *Nature* 485:242–245.
10. Sanders SJ, et al. (2012) De novo mutations revealed by whole-exome sequencing are strongly associated with autism. *Nature* 485:237–241.
11. De Rubeis S, et al.; DDD Study; Homozygosity Mapping Collaborative for Autism; UK10K Consortium (2014) Synaptic, transcriptional and chromatin genes disrupted in autism. *Nature* 515:209–215.
12. OMIM (Online Mendelian Inheritance in Man).; McKusick-Nathans Institute of Genetic Medicine; Johns Hopkins University, Baltimore.
13. The DDD Study (2015) Large-scale discovery of novel genetic causes of developmental disorders. *Nature* 519:223–228.
14. Basel-Vanagaite L, et al. (2012) Deficiency for the ubiquitin ligase UBE3B in a blepharophimosis-ptosis-intellectual-disability syndrome. *Am J Hum Genet* 91: 998–1010.
15. Basel-Vanagaite L, et al. (2014) Expanding the clinical and mutational spectrum of Kaufman oculocerebrofacial syndrome with biallelic UBE3B mutations. *Hum Genet* 133:939–949.
16. Flex E, et al. (2013) Loss of function of the E3 ubiquitin-protein ligase UBE3B causes Kaufman oculocerebrofacial syndrome. *J Med Genet* 50:493–499.
17. Kariminejad A, et al. (2017) Kaufman oculo-cerebro-facial syndrome in a child with small and absent terminal phalanges and absent nails. *J Hum Genet* 62:465–471.
18. Pedurupillay CR, et al. (2015) Kaufman oculocerebrofacial syndrome in sisters with novel compound heterozygous mutation in UBE3B. *Am J Med Genet A* 167A:657–663.
19. Yilmaz R, et al. (2018) Kaufman oculocerebrofacial syndrome: Novel UBE3B mutations and clinical features in four unrelated patients. *Am J Med Genet A* 176: 187–193.
20. Chahrour MH, et al.; ARRA Autism Sequencing Collaboration (2012) Whole-exome sequencing and homozygosity analysis implicate depolarization-regulated neuronal genes in autism. *PLoS Genet* 8:e1002635.
21. Kishino T, Lalande M, Wagstaff J (1997) UBE3A/E6-AP mutations cause Angelman syndrome. *Nat Genet* 15:70–73.
22. Froyen G, et al. (2008) Submicroscopic duplications of the hydroxysteroid dehydrogenase HSD17B10 and the E3 ubiquitin ligase HUWE1 are associated with mental retardation. *Am J Hum Genet* 82:432–443.
23. Küry S, et al. (2017) De novo disruption of the proteasome regulatory subunit PSMD12 causes a syndromic neurodevelopmental disorder. *Am J Hum Genet* 100: 352–363.
24. O'Roak BJ, et al. (2012) Sporadic autism exomes reveal a highly interconnected protein network of de novo mutations. *Nature* 485:246–250.
25. Sowa ME, Bennett EJ, Gygi SP, Harper JW (2009) Defining the human deubiquitinating enzyme interaction landscape. *Cell* 138:389–403.
26. Brosnan JT, Brosnan ME (2006) Branched-chain amino acids: Enzyme and substrate regulation. *J Nutr* 136(Suppl 1):207S–211S.
27. Novarino G, et al. (2012) Mutations in BCKD-kinase lead to a potentially treatable form of autism with epilepsy. *Science* 338:394–397.
28. Herring WJ, Litwer S, Weber JL, Danner DJ (1991) Molecular genetic basis of maple syrup urine disease in a family with two defective alleles for branched chain acyltransferase and localization of the gene to human chromosome 1. *Am J Hum Genet* 48:342–350.
29. White PJ, et al. (2018) The BCKDH kinase and phosphatase integrate BCAA and lipid metabolism via regulation of ATP-citrate lyase. *Cell Metab* 27: 1281–1293.e7.
30. Braganza A, et al. (2017) UBE3B is a calmodulin-regulated, mitochondrion-associated E3 ubiquitin ligase. *J Biol Chem* 292:2470–2484.
31. Ziegler AB, et al. (2017) Cell-autonomous control of neuronal dendrite expansion via the fatty acid synthesis regulator SREBP. *Cell Rep* 21:3346–3353.
32. Bernier R, et al.; Simons VIP consortium (2017) Developmental trajectories for young children with 16p11.2 copy number variation. *Am J Med Genet B Neuropsychiatr Genet* 174:367–380.
33. Steinman KJ, et al.; Simons VIP Consortium (2016) 16p11.2 deletion and duplication: Characterizing neurologic phenotypes in a large clinically ascertained cohort. *Am J Med Genet A* 170:2943–2955.
34. Balasubramaniam S, Duley JA, Christodoulou J (2014) Inborn errors of purine metabolism: Clinical update and therapies. *J Inherit Metab Dis* 37:669–686.